Atomistic comparison between stoichiometric and nonstoichiometric glasses: The cases of As_2Se_3 and As_4Se_4

Jun Li
Department of Physics and Astronomy, Condensed Matter and Surface Science Program, Ohio University, Athens, Ohio 45701-2979

D. A. Drabold
Trinity College, Cambridge, CB2 1TQ, United Kingdom
and Department of Physics and Astronomy, Ohio University, Athens, Ohio 45701
(Received 19 April 2001; published 23 August 2001)

A first-principles molecular dynamics study of glassy As_2Se_3 and As_4Se_4 is presented. We focus on the differences in local structure between these glasses and identify the structural elements of As_4Se_4 and present a model of the material in close agreement with experiments. We analyze the vibrational modes in both models in terms of excitations of the structural elements from which each glass is composed.

DOI: 10.1103/PhysRevB.64.104206 PACS number(s): 73.61.Jc, 61.43.Fs, 71.55.Jv, 63.50.+x

I. INTRODUCTION

Arsenic triselenide (As_2Se_3) has been extensively studied as a classic glass former in experiments. A basic interest of this system arises from its average coordination number (2.4), which is at a floppy to rigid transition threshold predicted by the theory of Phillips[1] and Thorpe.[2] Recently, novel and unique light-induced phenomena were observed in g-As_2Se_3 and g-As_4Se_4. Hisakuni and Tanaka[3] observed the photoinduced fluidity in chalcogenide glasses including As_2Se_3. Krecmer *et al.*[4] demonstrated optomechanical effects in As_4Se_4 (a direct mechanical signature of the polarization of light, so far observed only in this material). These experiments have aroused new interest in the As_xSe_{1-x} systems. An essential precursor to comprehending these effects in a complete microscopic fashion is to produce realistic and well characterized models of these glasses, and especially As_4Se_4 with its interesting optomechanical features. It is clear that there is an important role for theory here, since experiments always involve aggregates of atoms, and can offer limited insight into the local structure of the glass and the atomistic origins of photoinduced changes in structure.

This work offers insights into the nature of nonstoichiometric glasses. For multinary glasses there are special compositions which are strongly chemically preferred (in which no energetically unfavorable homopolar or ''wrong'' bonds occur). These compositions are called ''stoichiometric'' and are typically particularly good glass formers (As_2Se_3, SiO_2, and $GeSe_2$ are examples). In each of these examples, there are crystalline analogues of the glasses with the same local chemical order, and built from the same fundamental units (pyramids or tetrahedra in the case of the examples given). The existence of underlying ''building blocks'' for a particular composition is usually a considerable aid to modeling these complex materials, since these structures typically exist in glassy, solid and even liquid phases, at least not too far above the melting point.

For nonstoichiometric glasses (with composition intermediate between possible stoichometric glasses), the situation is far less clear. Two possibilities come to mind. In the first case one might expect a network to phase separate into multiple (stoichiometric) parts. Alternately a continuous random network (CRN) could be formed in which more complex building blocks (with composition consistent with the material) form a glass of more complex structure. We investigate this latter suggestion in this paper, and find that a CRN picture is suited to the nonstoichiometric glass As_4Se_4.[5] We compare this glass in detail with structural and vibrational measurements on the material. The importance of these ''building blocks'' has been emphasized in recent promising work on the glass transition of Kerner.[6] Some particularly interesting experimental work on rigidity transitions and the microstructure of non stoichimetric glasses has recently appeared. Georgiev and co-workers[7] have been able to infer the nature of the building blocks over a wide range of compositions by application of temperature modulated differential scanning calorimetry measurements. This data provides an important challenge for theories of the nonstoichiometric glasses.

Experimentally, it is believed that the structure of As_xSe_{1-x} systems exhibits a continuous change with increasing arsenic concentration (x).[8] According to experiments on the viscosity, glass transition temperature, and magnetic susceptibility, at low arsenic concentration ($x<10\%$), the structure is composed primarily of branched selenium chains. Only after x reaches 20%, pyramidal $AsSe_3$, develops into a dominant structural component in the network and is the sole ''building block'' at the stoichiometric composition As_2Se_3 ($x=40\%$), except for some defects. Experiments on As_xSe_{1-x} systems have confirmed that on average As has three nearest neighbors and Se has two no matter what the arsenic concentration. In other words, one can view the As-Se network to be composed of trinodes (X) and binodes (Y). In principle, tribonded As atoms occupy the top X position of the pyramid while the Se atom on the corner Y position which bridges two pyramids together. Thus, the network of As_2Se_3 would be built upon a pure energetically favored heteropolar As-Se bond. With the As concentration x exceeding 40%, the stoichiometric balance breaks between As and Se. There is an insufficient number of Se atoms available for the excess As atoms, and the corresponding building

block can no longer be soley the pyramidal XY_3 configuration. There will always be at least one As atom in the neighborhood of some As sites, i.e., the network must include homopolar As-As bonds. The concentration of nodes and bonds is the primary global parameter of the structure in the network. For a network satisfying the 8-N rule, at least 20% bonds must be As-As bonds in As_4Se_4. In addition to the bond property changing in the network frame, the trinode X population increases 10% in As_4Se_4 over As_2Se_3.

This paper is the first part of our effort to reveal the nature of the disordered As_xSe_{1-x} systems on the microscopic scale. We will focus on the structural and dynamical properties of both As_2Se_3 and As_4Se_4 in this paper and leave the details of electronic structure and photostructural simulation to a later work. A thorough comparison between the theoretical approach and experiments has been made on g-As_2Se_3 in our recent work,[9] which gave a uniform agreement with the experiments on the structure, vibration, and electronic properties of g-As_2Se_3. Then, further simulation was employed to unfold the atomistic photoresponse.[10] Our emphasis here is on the comparison between the g-As_2Se_3 and g-As_4Se_4 from our theoretical models. Where experimental data is available, we will also give a convenient comparison between our g-As_4Se_4 model and corresponding experiments. In the next section, we outline the approach to model generation. Section III focuses on the structural characteristics. Our attention is focused on the building block and the statistics of the network. Both the short range order (SRO) and intermediate range order (IRO) are discussed with the changes in the ring structures. Dynamics is analyzed in Sec. IV, where the effects of increasing As concentration on the vibrational modes are revealed. Finally, a summary is made in Sec. V with some further discussion.

II. MODEL GENERATION

An approximate first-principles type molecular-dynamics (MD) program, FIREBALL96,[11] was used throughout the calculation. In this method the Harris functional within the local density approximation is used in a scheme with the mathematical structure of nonorthogonal tight-binding,[12] and the use of no free parameters in constructing the Hamiltonian matrix. This scheme does very well at producing experimentally credible models because of its nearly unique balance between accuracy and efficiency. We also performed further calculations by using a more complete and sophisticated first-principles program SIESTA.[13] It turns out that the result of FIREBALL96 is not inferior to the best result of SIESTA using a rich basis set.

Because of the very short times scales one is compelled to employ in *ab initio* MD simulations, it is impossible to do anything similar to a complete exploration of configuration space. A trivial *reductio ad absurdum* makes the point; one could attempt to make a model of a binary glass by putting all the atoms of one species in one side, and the others on the other side of a supercell. Quite obviously, for a model involving hundreds of atoms, a picosecond time scale would fail miserably for creating a homogenous model. It is important to note clearly that the procedure we follow here is *not* a direct simulation of the laboratory process of glass formation, but it is no more unreasonable than any other successful approach. The test of any new model is uniform agreement with experiments, which we discuss later in the paper.

Thus, as usual,[14] we advocate using *a priori* information, in this case starting with a large cubic supercell of crystalline As_4Se_4 (Ref. 15) rescaled to the experimental glass density. This procedure ensures reasonable chemical order from the beginning. We then melt the cell at 2000 K and maintain it there for 2 ps (a time sufficient to make the system lose memory of the starting topology). After the cell lost its initial ordered structure, we began quenching it down to about 700 K over 4 ps. We fixed the cell temperature with Gaussian constrained dynamics at 700 K for 2 ps to let the atoms equilibrate slightly above the glass transition temperature. Then we let the cell fall to 300 K and maintained this for 2 ps. At the final step, we steepest descent quenched the cell to 0 K.

We found that the above procedure could generally create a ''coarse'' model, being good on the large scale (>6Å). A regime of extended annealing improved the structure at the second nearest neighbor scale ($3-6$ Å). A final simulation of 4 ps free (nondissipative) dynamics even at low temperatures (<100 K) would give a model in good and consistent agreement with electronic, vibrational, and structural measurements. It is fair to note that our use of a starting model with uniform chemical order over a several Å scale implies that our final network will be relatively homogeneous. Thus, we cannot expect to model phase separation well, though this is not expected to be important for the As_4Se_4 glass we focus on here.

All the calculations were performed at constant volume using the Γ point to sample the Brillouin zone. Considering the large supercell volume it was reasonable to use Γ point alone. The final model of g-As_2Se_3 consists of 86 arsenic atoms and 129 selenium atoms with the side length 18.50 Å, and g-As_4Se_4 has 256 atoms in total with the side length 19.38 Å.

III. STRUCTURAL PROPERTIES

In the ordered states, the structures of As_2Se_3 and As_4Se_4 are very distinct. Crystalline As_2Se_3 has a layered structure based on the $AsSe_3$ spiral chain, while the crystal As_4Se_4 is built from molecular As_4Se_4, which consists of the building block Se_2As-$AsSe_2$. However, the situation changes in the disordered states. Both the bond length and bond angle spread over a wide range. The building blocks emerge with high diversity and flexibility in inter-block bonding. The longer-range order associated with the $AsSe_3$ spiral chain and molecular As_4Se_4 disappear from the disordered states. Structural information can be extracted from the interference function $F(Q)$ measured in scattering experiments. The topology of the glasses can be described (incompletely) by the pair correlation function $G(r)$, which is related to $F(Q)$ by $F(Q)=\int_0^\infty G(r)\sin Qrdr$, where $Q=4\pi\sin\theta/\lambda$. The integration to infinity in $F(Q)$ was truncated at radial distance R_c in the practical calculation so that no more than half of the side length of the supercell is included. $G(r)$ was defined as

TABLE I. Basic short range order parameters in models g-As_2Se_3 and g-As_4Se_4 and compared to available measurements. r_1 is the average bond length, C. N. the average coordination number, and r_2 the second nearest neighbor distance.

	r_1 (Å)		C. N.		r_2 (Å)	
	Models	Exp.	Models	Exp.	Models	Exp.
As_2Se_3	2.46	2.41–2.44	2.40	2.4–2.44	3.70	3.66–3.69
As_4Se_4	2.47	2.41–2.45	2.50	2.5–2.55	3.82	3.73

$G(r)=4\pi r[\rho(r)-\rho_0]$, where ρ_0 is the average density and $\rho(r)$ the density function for pairs separated by distance r. We will discuss the detailed structure features according to the length scale naturally emerging from the $G(r)$.

A. Short range order

The scale of SRO is not longer than the second nearest neighbor distance in our definition. The parameters closely studied include bond length, bond angle, coordination number, etc. Table I gives an overview of the SRO in g-As_2Se_3 and g-As_4Se_4. The average bond length and average coordination number closely agree with the available measurement.[16] With the As concentration increasing, the average coordination number increases to 2.5 in g-As_4Se_4 from 2.4 in g-As_2Se_3. Also listed is the second nearest neighbor distance [Y-Y, contributing to the second peak in $G(r)$, see below]. The agreement with experiment is very good. Notably, the longer Y-Y distance in As_4Se_4 vs As_2Se_3 is also reproduced very well by the models. The SRO is a well defined property only statistically. For example, for a typical valence alternation pair (VAP,[17]) the overcoordinated (Se_3) and undercoordinated (Se_1) pair, will not change the observed SRO at the resolution of ordinary experiments. Neither will the compensated wrong bond pairs.

As in real materials, both models contain structural defects. In addition to the normally coordinated As_3 and Se_2, the VAPs; Se_1 and Se_3, are significant in both models. Table II summarizes the statistical distribution of the main structural components. In both models, the coordination defects of As are rare while Se atoms show a strong tendency to form VAPs. Almost 40% Se formed into the VAPs in both models. The higher coordination defect concentration of Se over As indicates that the As coordination defects are very energetically unfavored relative to the comparatively attractive ''VAP option'' for Se. This might account for the larger change of the first shell of As_2Se_3 at the Se K edge than at the As K edge seen from EXAFS during irradiation.[18]

One needs to carefully ascertain the role played by the homopolar bond As-As in the nonstoichiometric As_4Se_4 system. Once the concentration x is given, under the 8-N rule, the global rate of homopolar bonding is fixed by simple algebra, which gives zero rate for the stoichiometric As_2Se_3 and 20% for the nonstoichiometric As_4Se_4 system. The homopolar bond is called traditionally ''wrong bond'' in As_2Se_3, since any homopolar bond is unnecessary in an ideally bonded glass. In this sense, that portion of As-As bonds in Table II can be counted as wrong bonds if over the global rate for a given composition. In As_2Se_3, one can interpret the wrong bond as the result of composition density fluctuation, i.e., network inhomogeneity. The existence of wrong bonds has been observed in the real g-As_2Se_3.[19] $10-15\%$ homopolar bonds in the evaporated As_2Se_3 films were estimated by the extended x-ray absorption fine structure experiment with an error bar $\pm 10\%$. For the well-annealed bulk As_2Se_3, the rate of wrong bonds was expected to be lower.[20] Table II shows that pairs of both the coordination defect and wrong bonds compensate each other. The As_4Se_4 model contains only about 6% wrong bonds pairs, less than about 11% in the As_2Se_3 model. In this sense, the quality of the As_4Se_4 model should be a little better in the chemical order than that of the As_2Se_3 model.

We found that about 60.9% atoms in the As_2Se_3 model could be attributed to the pyramidal configuration $AsSe_3$ and about 70.3% atoms in the As_4Se_4 model belonged to the configuration As-$AsSe_2$ (Fig. 1). We found that most of the remaining atoms in As_2Se_3 model had the form of As-$AsSe_2$ and most of the residual atoms in As_4Se_4 had the form of $AsSe_3$. Should one count the chemical perfect configuration $AsSe_3$ as a ''defect'' in As_4Se_4 since the local chemical environment of $AsSe_3$ conflicts with the global stoichiometric requirement? To avoid generalizing the meaning of ''defect'' and recognizing the difficulty of terminology, we adopt multiple building blocks according to the local chemical environment. We label those regions with extra As-As bonds ''As rich'' and Se-rich regions those volumes in which only As-Se bonds are present. It is obvious that the dominant building block is determined by the global stoichiometry, and becomes the backbone of the network. It is of considerable interest that to a large degree, only two such building blocks emerge in the As_4Se_4 material.

In As_2Se_3 model, the bond length distributes over the range $2.34-2.63$ Å and in As_4Se_4, the range is $2.33-2.63$ Å. The structural unit disorder (strain disorder of building blocks) is demonstrated by the wide distribution in bond length and bond angle, enhancing the flexiblity of the interblock connections. Table III gives the average bond

TABLE II. The statistical distribution of the main structural components in g-As_2Se_3 and g-As_4Se_4 models. Percentage of a given component in the total configuration is given in parentheses. Here the subscript number indicates the coordination number. For example, As_3 means the three-bonded As sites.

	As_3	Se_2	Se_1	Se_3	As-Se	As-As	Se-Se
As_2Se_3	83 (96.5%)	78 (60.5%)	26 (20.2%)	25 (19.4%)	199 (77.1%)	30 (11.6%)	29 (11.2%)
As_4Se_4	126 (98.4%)	72 (56.3%)	29 (22.7%)	27 (21.1%)	218 (68.1%)	84 (26.3%)	18 (5.6%)

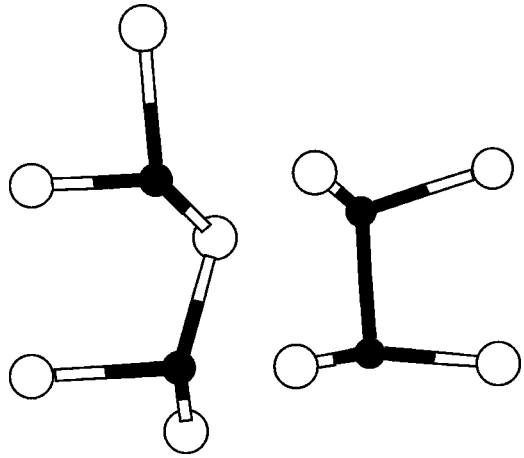

FIG. 1. The basic building blocks in the g-As_2Se_3 and g-As_4Se_4 models. The small black sphere is arsenic atom and the large white sphere a selenium atom. The left part is two neigbored pyramidal $AsSe_3$ and the right is a unit of Se_2As-$AsSe_2$. In our model, about 60.9% atoms in the As_2Se_3 could be attributed to the configuration $AsSe_3$ and about 70.3% atoms in the As_4Se_4 model belonged to the configuration As-$AsSe_2$, most of which are a part of the unit Se_2As-$AsSe_2$.

angles around three-bonded As sites, three- and two-bonded Se sites in As_2Se_3 and As_4Se_4, and compared to the crystalline bond angles.[15] The average bond angles in the disordered states are not so different as in the ordered states. Figure 2 gives the detailed bond angle distribution. It is obvious that the bond angles are centered near the corresponding crystalline bond angle, confirming the existence of ''building blocks,'' with a significant broadening effect due to the structural unit disorder of the building blocks. Figure 2(a) shows that bond angles around the three-bonded As sites have a slightly wider range in g-As_4Se_4 than in g-As_2Se_3. The bond angles of three-bonded As sites demonstrate a strong tendency to concentrate from 90° to 105° in line with the features of the corresponding crystalline bond angle distribution,[15] while bond angles of three- and two-bonded Se sites do not have strong peaks over a broad range from 85° through 115° as in crystalline structures. The broader distribution of bond angles around As and Se confirms once again that Se is superior to As in its flexibility for insertion into the disordered network.

With the increasing population of trinodes in the As_4Se_4 network, one can expect a more intricate structure than in g-As_2Se_3. This conclusion is verified by a dramatic change in the ring statistics (Table IV). The number of small rings

TABLE III. Average bond angles in g-As_2Se_3 and g-As_4Se_4 models, compared to corresponding crystalline structures. The meaning of subscript number is the same as in Table II.

	As_3		Se_3		Se_2	
	Models	Cry.	Models	Cry.	Models	Cry.
As_2Se_3	98.8°	99.7°	99.0°		101.4°	94.4°
As_4Se_4	98.5°	98.1°	100.1°		100.7°	99.3°

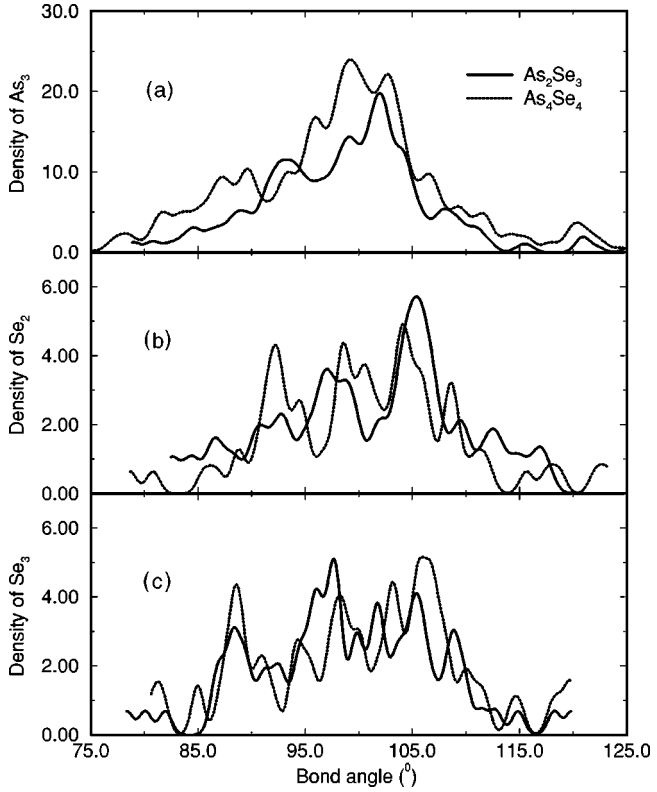

FIG. 2. Bond angle distribution in g-As_2Se_3 and g-As_4Se_4 models around (a) the three-bonded As sites, (b) the two-bonded Se sites, and (c) the three-bonded Se sites.

(less than six-membered ring) is almost doubled in g-As_4Se_4. They are fundamentally a SRO structure, which is sensitive to the population of trinodes in the networks. The five-membered rings are the most popular SRO rings in both As_2Se_3 and As_4Se_4. Molecular As_4Se_4 has five-membered rings, which can be seen as a signature of homopolar As-As bonds. Both the As_2Se_3 and As_4Se_4 are composed of the building blocks $AsSe_3$ and As-$AsSe_2$ with different ratios. Direct inspection of the atomistic arrangement of the five-membered rings confirmed that most of the local configurations have the unit As-$AsSe_2$, although occasionally there are few five-membered rings containing no As-As bonds,[9] which in general are related to specific structures and are not common in either As_2Se_3 or As_4Se_4. The abundance of five-membered ring could be used as an signature of As-rich regions. All structural characterizations reported in this paper are for the zero temperature model; we do not expect thermal effects to broaden these results significantly.

B. Intermediate range order

Fundamentally, the intermediate range order is a topic concerned with the connectivity among the structural build-

TABLE IV. Ring statistics. The number of n-membered rings, $n=3$ through $n=12$.

Ring size	3	4	5	6	7	8	9	10	11	12
As_2Se_3	2	3	11	4	5	5	2	3	2	6
As_4Se_4	5	8	16	8	8	9	11	6	9	2

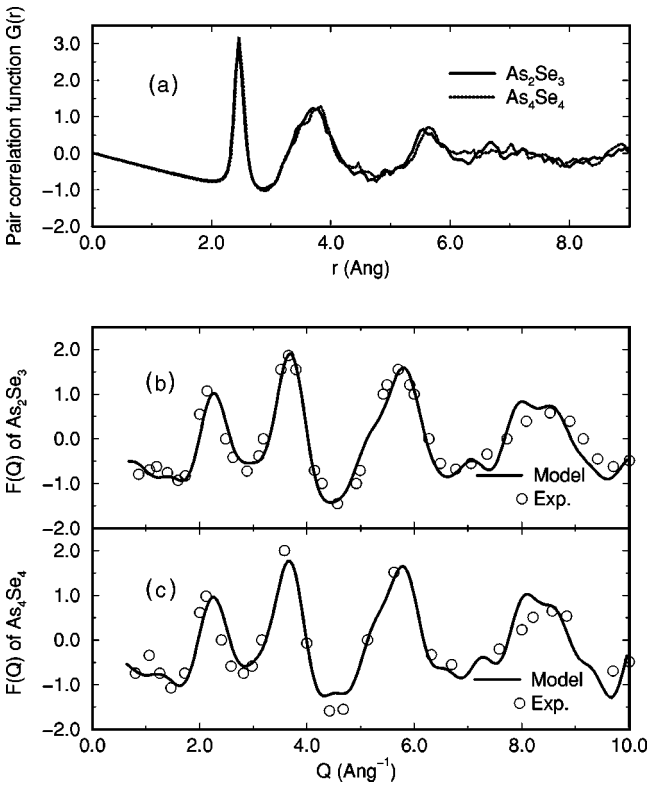

FIG. 3. Reduced pair correlation functions (a) and inference functions (b) of g-As_2Se_3 and g-As_4Se_4. Experimental inference function (Ref. 8) is given for comparison with model.

ing blocks. It is generally related to the structural features beyond the second peak in the pair correlation function $G(r)$. Figure 3(a) shows $G(r)$ of g-As_2Se_3 and g-As_4Se_4. The small difference between the $G(r)$ of g-As_2Se_3 and g-As_4Se_4 agrees with the trend observed in experiment (refer to Fig. 4 in Ref. 8). Significant differences occur only after the third peak in $G(r)$, after about 6.5 Å, which was found to be the minimium distance to give the first sharp diffraction peak (FSDP) in the interference function $F(Q)$ in our calculation (we found that the calculated FSDP first occurred at about the measured position of 1.3 $Å^{-1}$ as the truncated R_c reached about 6.5 Å in both models). Direct inspection of the microscopic geometry indicates that the correlation between two pyramids sharing a common corner dominates on that length scale and is therefore salient to the FSDP. This nodal correlation has a seesaw arrangement of X as -X-Y/X-X-, which gives a strong contribution to the nine-membered ring population. However, as the truncated R_c extended to the model limit (half of the side length of the supercell) the agreement deteriorated much more in the As_2Se_3 model than in the As_4Se_4 model. Figures 3(b) and 3(c) give the direct comparison with the experiment on $F(Q)$ for As_2Se_3 and As_4Se_4, respectively. The agreement between models and experiments is impressive for both As_2Se_3 and As_4Se_4. However, the FSDP position of As_4Se_4 model is slightly closer to its experimental position than the As_2Se_3 model is.

In the IRO range, we found that the seesaw arrangement of X has a strong correlation with the FSDP. A similar study of g-$GeSe_2$ found that the edge-sharing Ge is strongly correlated to the FSDP.[21,22] In both systems, the correlation is arising from the two neighboring building blocks. In As_xSe_{1-x} systems, the building block is pyramidal or closely related As-$AsSe_2$, while in $GeSe_2$ it is tetrahedra. This correlation pattern debuts in the nine-membered rings. We found that the nine-membered rings are the second most popular ring pattern in As_4Se_4. The large difference in the number of nine-membered rings may partly account for the reason why the position of FSDP is slightly closer to the experimental position in the As_4Se_4 model than in the As_2Se_3 model, since the As_4Se_4 model contains more correlation patterns associated with the FSDP. The other interesting ring pattern is the 12-membered ring, which is the unique ring structure of the layers of the crystal As_2Se_3. However, the number of 12-membered rings in g-As_4Se_4 become rather small comparing to g-As_2Se_3. This indicates that large ordered fragments of $AsSe_3$ cannot survive with the excess As concentration.

IV. DYNAMICAL PROPERTIES

The dynamical properties are characterized by the vibrational density of states (VDOS). The calculation method has been described in previous work.[21] A thorough comparison with experiments and molecular model calculations has been made on g-As_2Se_3 models.[9] Since the experimental data of the VDOS of g-As_4Se_4 is not available to us, we focus on the theoretical-comparison between g-As_2Se_3 and g-As_4Se_4 instead. Emphasis is given to correlating the vibrational spectra with the dynamics of the main building blocks.

The general features of VDOS are compared in Fig. 4. Both g-As_2Se_3 and g-As_4Se_4 consist of two main bands. The lower-energy band (LEB) goes up to 150 cm^{-1} and the higher-energy band (HEB) decays after 300 cm^{-1}. The vibrational modes in LEB is strongly correlated to the connectivity of the network,[23] consisting of extended interblocks vibrations, in analogy with acoustic modes. The vibrational modes in HEB tend to strongly depend on the configurations of the building blocks, consisting of much more localized intrablock vibration: optical-like modes. Approaching the two band edges of HEB, the vibrations become much more localized on a few atomic groups, making it possible to distinguish the origin of the vibration in terms of the building blocks. In contrast, microscopic identification for the modes in LEB is difficult as they are quite spatially extended. It is clear in Fig. 4 that both bands LEB and HEB of As_4Se_4 shift upward relative to those of As_2Se_3. However, the shift of HEB is much bigger than that of LEB. This relative shift of VDOS between As_2Se_3 and As_4Se_4 is due to the change of the dominant building blocks. The effective valence force field undergoes a global change with the increasing of As concentration. However, the sutble effects of As concentration become visible only by suitable analysis as below.

Since the SRO is a well defined property of glasses, we can analyze the vibrational modes according to the local atomistic configuration to reveal the statistical relation between the topological units and the dynamics. From the structural analysis in previous section, we established a tentative relation between the building block and the As concentration. In

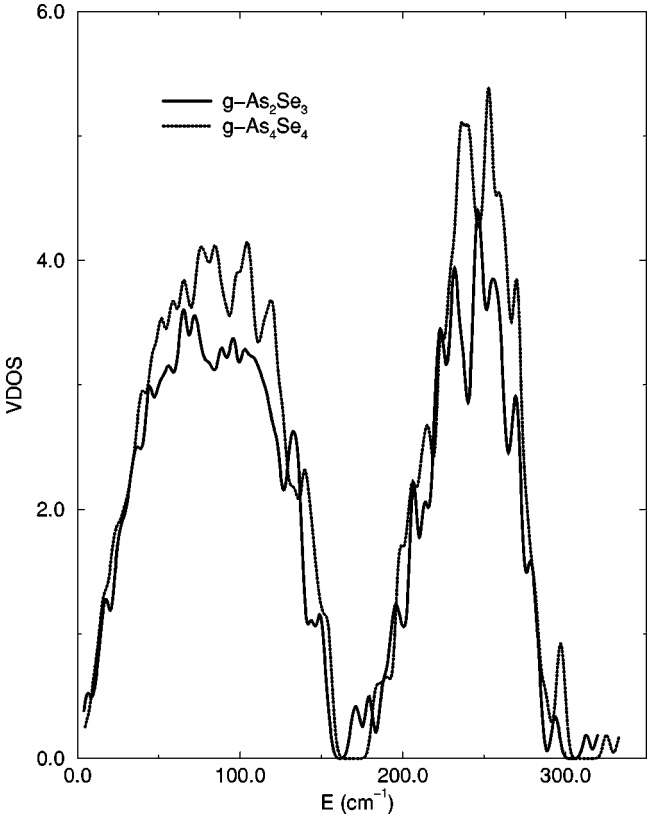

FIG. 4. Calculated vibrational density of states for g-As_2Se_3 and for g-As_4Se_4.

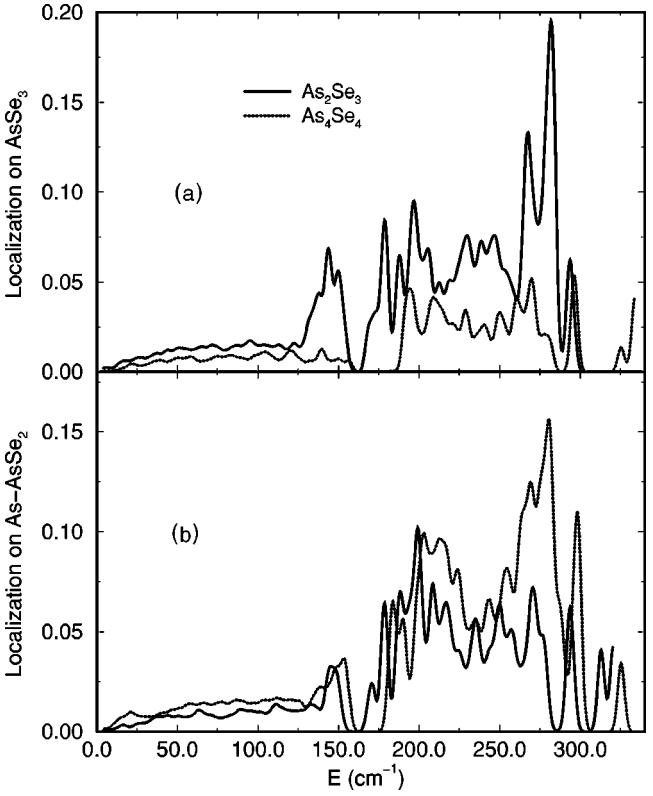

FIG. 5. Projected localization of vibrational modes on the configuration (a) $AsSe_3$ pyramid as in "ideal" g-As_2Se_3 and (b) As-$AsSe_2$ (important structural unit in g-As_4Se_4.)

the Se-rich region, the main building block adopts the pyramid structure $AsSe_3$, while in the As-rich region, within the nearest neighborhood, the building block has a form, As-$AsSe_2$. We found that by these two structural units we had been able to describe systematically and connect to the vibrational modes of As_2Se_3 and As_4Se_4.

In an ideal pyramid configuration XY_3,[24] there are four fundamental vibrational modes. In terms of symmetry group C_{3v}, they are the symmetrical and anti-symmetrical bond-stretching modes, i.e., γ_1 and γ_3, respectively, and two bond-bending modes, i.e., γ_2 and γ_4, respectively. All these modes are infrared and Raman active. Experiments[25] on g-As_2Se_3 assigned γ_2 and γ_4 modes in the range [50,150] in cm^{-1}, belonging to our LEB, and γ_1 and γ_3 modes in the range [150,300] in cm^{-1}, corresponding to our HEB. Our calculation coincides with the spectral identification.

The bond-bending modes, in which the bridging Se atoms move opposite to the As atoms, admix into interblock vibrational modes, developing into extended modes in the LEB. On the other hand, the As-Se stretching modes feature intrablock vibrational modes, tending to have a higher localized character in the HEB, especially when approaching the edge of HEB. Molecular model[26,27] and valence force field[28] calculations indicated that γ_3 mode was at 220 cm^{-1} and γ_1 at 227 cm^{-1} for the $AsSe_3$ configuration and the the symmetric stretching frequency of the Se chain could be at 268 cm^{-1}. These model calculations qualitatively agreed with our identification on the spectra of vibrational modes in g-As_2Se_3.[9] The building block XY_3 and Y_2X-XY_2' gave a strong contribution in the lower HEB (<250 cm^{-1}). And the localized modes in the upper HEB (>250 cm^{-1}) were strongly related to the rings or chains. The character of the vibrational modes are essentially the same in g-As_4Se_4. However, due to the increase of As concentration, the dominant building block changes from XY_3 to X-XY_2.

To distinguish the vibrational modes in As_4Se_4, we projected the inverse participation ratio[21] of vibrational modes according to the two congifurations $AsSe_3$ and As-$AsSe_2$. Figure 5(a) illustrates the contribution of the configuration $AsSe_3$ to the vibrational spectra. Because of differences in the environment beyond the immediate vicinity of the units, there are variations in the modes compared to As_2Se_3. For example, the localized modes at the high edge of LEB (~ 150 cm^{-1}) and the low edge of HEB (~ 175 cm^{-1}) in As_2Se_3, which are strongly related to some specific defect structures in As_2Se_3 model, disappear in As_4Se_4. Comparable modes have the largest shift ~ 7 cm^{-1} in the lower HEB and exhibit a small shift ~ 3 cm^{-1} in the higher HEB, where the corresponding $AsSe_3$ units become parts of rings or chains structures. The trend is the same for the vibrational modes from the configuration As-$AsSe_2$ [Fig. 5(b)]. The relative shift for the comparable structural units is largest in the lower HEB and become small as approaching the higher HEB. Specific modes from uncommon (defect) structures disappear either in As_2Se_3 or in As_4Se_4.

The two most localized modes around ~ 275 cm^{-1} in Fig. 5 are worthy of additional discussion. This pair of

modes originates from the inter-block mode of vibration by the bridging Se between the main building blocks, having the chain topology: *X*-Se-*X*. Experiments on the temperature dependence of vibrational spectra of As_2Se_3 at the room temperature proposed the measured modes at 269 and 277 cm^{-1} belonged to the bridging Se chain modes.[29] Our calculation gives the pair of bridging Se modes at 267.6 and 281.8 cm^{-1} for the building block $AsSe_3$ and 269.4 and 280.5 cm^{-1} for the building block As-$AsSe_2$. The small and uneven shifts between the pair of localized modes reflect the difference of the building blocks over the bridging Se chains in As_2Se_3 and As_4Se_4.

V. SUMMARY AND DISCUSSION

We studied the structure and dynamics of g-As_2Se_3 and g-As_4Se_4 by first-principles MD calculation. We built our models using previously established techniques. A longer annealing process and bigger size can generally lead to a better model containing few structure defects. However, a realistic model (meaning that it agrees reasonably well with all experiments) depends on experience and patience to a degree. All our statistical analysis or discussion are performed on our well-annealed models by MD simulation. An interesting point is that even though the rate of wrong bonds in the As_4Se_4 model are reduced by almost a factor of 2 relative to the As_2Se_3 model, the VAP concentration is almost unchanged in the two As_xSe_{1-x} models. This suggests that the VAPs are somehow a fundamental ingredient of the As_xSe_{1-x} systems, while the wrong bonds are of course composition dependent.

A hierarchy of disorders, network inhomogeneity, structural unit disorder, and the structural defect, naturally emerges from our models. The distinct building blocks demonstrates the composition disorder in the multinary system, which involves an intrinsic composition inhomogeneity on a very short length scale. The most popular type of building block must be determined by the global stoichiometry and determines the general properties of the disordered systems. For example, in our two As_xSe_{1-x} systems ($x \geqslant 40\%$), we assigned the pyramid $AsSe_3$ for Se-rich regions and the unit As-$AsSe_2$ or Se_2As-$AsSe_2$ to As-rich regions. As x approaches the stoichiometric density, the pyramid $AsSe_3$ becomes the dominant structural unit. Once the As concentration exceeds the stoichiometric composition, the building block As-$AsSe_2$ or Se_2As-$AsSe_2$ becomes important and is the overwhelming unit as x approaches 50% in As_4Se_4. We noted that the multiple building blocks were also observed in other multinary systems, for example, GeAsSe ternaries.[30]

The role of defects depends on the detailed configuration. The VAPs of Se are one of the major defects, in which electrons are proposed to energetically benefit from the local distortions. We have always noted that the miscoordinated As, though it is a minor defect in both models, leads to electronic gap states, so this would seem to agree with the experiments that there is a clean (state free) optical gap. We will discuss the electronic properties elsewhere.

The ring structure has been used in our analysis as an indicator of some specific structural patterns. For example, the five-membered rings convey information about the nonstoichiometric distribution of elements in the SRO range. From the direct inspection, we defined the As - and Se-rich regions to simplify our discussion. However, note that the terms of As - and Se-rich regions are confined in the SRO range and have nothing with the macroscopic phase separation. The nine-membered rings suggest a correlation between the neighboring building blocks sharing corners may be a strong candidate for microscopic origin of the FSDP. This is in contrast to earlier suggestions[31–33] that the FSDP was arising from either the molecular structure or the remnant of crystalline layer of As_2Se_3. With the increase of As concentration, the tribonded sites grow up in the network. As a result, the number of ring structures increases dramatically from As_2Se_3 to As_4Se_4.

Beyond the stoichiometric composition of g-As_2Se_3, some of the heteropolar As-Se bonding is replaced by the homopolar As-As bond. The As-As bonds become an important factor in the dynamics of As_xSe_{1-x} materials. The higher concentration of As-As bonds impacts the global effective force field and induces a global shift between all the comparable vibrational modes. Another interesting relative shift is observed between comparable bridging Se modes, which indirectly reflects the difference between the building blocks $AsSe_3$ and As-$AsSe_2$.

Our work is limited in the sense that we can only advance a pair of models in this paper because of the computational expense in forming such models. However, since we used the same program to construct the glassy models and the model generation processes did not follow exactly the same path, but the self-consistent results were achieved in the two models, it is reasonable to take our results as a general representative of the corresponding properties of the real glasses. The self-consistency between two different models is an encouragement to the following study of the electronic properties and photostructural response.

ACKNOWLEDGMENTS

This work was supported in part by the National Science Foundation under Grant Nos. DMR 00-74624 and DMR 00-81006. We thank Professor Punit Boolchand, Professor Himanshu Jain, Mr. Gang Chen, and Professor Normand Mousseau for helpful discussions. D.A.D. thanks Trinity College, Cambridge for financial support.

[1] J.C. Phillips, J. Non-Cryst. Solids **43**, 37 (1981).
[2] M.F. Thorpe, J. Non-Cryst. Solids **57**, 355 (1983) .
[3] H. Hisakuni and K. Tanaka, Science **270**, 974 (1995).
[4] P. Krecmer *et al.*, Science **277**, 1799 (1997).

[5] One could suppose that As_4Se_4 is stoichiometric, but only for a *molecular solid* with nonbonded interactions between As_4Se_4 molecules. Glassy As_4Se_4 does not consist significantly of As_4Se_4 molecules and can therefore be considered non-

stoichiometric.
[6] R. Kerner, in *Properties and Applications of Amorphous Materials*, edited by M.F. Thorpe and L. Tichy (Kluwer, Dordrecht, 2001), p. 177.
[7] D.G. Georgiev, P. Boolchand, and M. Micoulaut, Phys. Rev. B **62**, R9228 (2000).
[8] A.L. Renninger and B.L. Averbach, Phys. Rev. B **8**, 1507 (1973).
[9] J. Li and D.A. Drabold, Phys. Rev. B **61**, 11 998 (2000).
[10] J. Li and D.A. Drabold, Phys. Rev. Lett. **85**, 2785 (2000).
[11] A.A. Demkov, J. Ortega, O.F. Sankey, and M. Grumbach, Phys. Rev. B **52**, 1618 (1995).
[12] O.F. Sankey and D.J. Niklewski, Phys. Rev. B **40**, 3979 (1989); O.F. Sankey, D.A. Drabold, and G.B. Adams, Bull. Am. Phys. Soc. **36**, 924 (1991).
[13] D. Sanchez-Portal, P. Ordejón, E. Artacho, and J.M. Soler, Int. J. Quantum Chem. **65**, 453 (1997).
[14] D.A. Drabold, S. Nakhmanson, and X. Zhang, in *Properties and Applications of Amorphous Materials*, edited by M.F. Thorpe and L. Tichy, Vol. 9 of *NATO Science Series II: Mathematics, Physics and Chemistry*, (Kluwer, Dordrecht, 2001), pp. 221–250.
[15] A.L. Renninger and B.L. Averbach, Acta Crystallogr., Sect. B: Struct. Crystallogr. Cryst. Chem. **29**, 1583 (1973).
[16] Y. Sagara, O. Uemura, S. Okuyama, and T. Satow, Phys. Status Solidi A **31**, 33 (1975).
[17] P.W. Anderson, Phys. Rev. Lett. **34**, 953 (1975); R.A. Street and N.F. Mott, *ibid.* **35**, 1293 (1975); Marc Kastner, David Adler, and H. Fritzsche, *ibid.* **37**, 1504 (1976).
[18] G. Chen and H. Jain (private communication).
[19] R.J. Nemanich, G.A.N. Connell, T.M. Hayes, and R.A. Street, Phys. Rev. B **18**, 6900 (1978).
[20] P. Boolchand (private communication).
[21] M. Cobb, D.A. Drabold, and R.L. Cappelleti, Phys. Rev. B **54**, 12 162 (1996).
[22] X. Zhang and D.A. Drabold, Phys. Rev. B **62**, 15 695 (2000).
[23] N. Mousseau and D.A. Drabold, Eur. Phys. J. B **17**, 667 (2000).
[24] G. Herzberg, *Infrared and Raman Spectra of Polyatomic Molecules* (Van Nostrand-Reinhold, New York, 1945).
[25] I.G. Austin and E.S. Garbett, Philos. Mag. **23**, 17 (1971).
[26] G. Lucovsky, Phys. Rev. B **6**, 1480 (1972).
[27] G. Lucovsky and R.M. Martin, J. Non-Cryst. Solids **8-10**, 185 (1972).
[28] P.J.S. Ewen, M.J. Sik, and A.E. Owen, in *The Structure of Non-Crystalline Materials*, edited by P.H. Gaskell and E.A. Davis (Taylor and Francis, London, 1977), p. 231.
[29] T. Arai, S. Komiya, and K. Kudo, J. Non-Cryst. Solids **18**, 289 (1975).
[30] Y. Wang, P. Boolchand, and M. Micoulaut, Europhys. Lett. **52**, 633 (2000).
[31] J.P. De Neufville, S.C. Moss, and S.R. Ovshinsky, J. Non-Cryst. Solids **13**, 191 (1973).
[32] J. Chang and D.B. Dove, J. Non-Cryst. Solids **16**, 72 (1974).
[33] A.J. Leadbetter and A.T. Apling, J. Non-Cryst. Solids **15**, 250 (1974).